nanomaterials

MDPI

Article

Adsorption Geometry of Alizarin on Silver Nanoparticles: A Computational and Spectroscopic Study

Cristina Gellini *, Marina Macchiagodena and Marco Pagliai *

Dipartimento di Chimica "Ugo Schiff", Università degli Studi di Firenze, via della Lastruccia 3–13, 50019 Sesto Fiorentino, Italy; marina.macchiagodena@unifi.it

* Correspondence: cristina.gellini@unifi.it (C.G.); marco.pagliai@unifi.it (M.P.)

Abstract: The knowledge of the adsorption geometry of an analyte on a metal substrate employed in surface enhanced Raman scattering (SERS) spectroscopy is important information for the correct interpretation of experimental data. The adsorption geometry of alizarin on silver nanoparticles was studied through ab initio calculations in the framework of density functional theory (DFT) by modeling alizarin taking into account all the different charged species present in solution as a function of pH. The calculations allowed a faithful reproduction of the measured SERS spectra and to elucidate the adsorption geometry of this dye on the silver substrate.

Keywords: alizarin; Raman spectroscopy; SERS; silver nanoparticles; DFT calculations

check for updates

Citation: Gellini, C.; Macchiagodena, M.; Pagliai, M. Adsorption Geometry of Alizarin on Silver Nanoparticles: A Computational and Spectroscopic Study. *Nanomaterials* **2021**, *11*, 860. https://doi.org/10.3390/nano11040860

Academic Editor: Ronald Birke

Received: 22 February 2021
Accepted: 25 March 2021
Published: 27 March 2021

Publisher's Note: MDPI stays neutral with regard to jurisdictional claims in published maps and institutional affiliations.

Copyright: © 2021 by the authors. Licensee MDPI, Basel, Switzerland. This article is an open access article distributed under the terms and conditions of the Creative Commons Attribution (CC BY) license (https://creativecommons.org/licenses/by/4.0/).

1. Introduction

Anthraquinone derivatives are chemical species used as dyes or lakes in textiles and paintings from ancient Egyptians until today [1–6]. These substances can be easily obtained from plants, such as alizarin and purpurin extracted from rubia tinctorum, or insects, such as carminic and kermesic acids obtained from cochineal. Art historians, curators, researchers, and restorers have determined the presence of these substances in works of art and cultural heritage by means of various techniques [2,5,7–9], including Raman spectroscopic analysis [9–15]. Among these organic dyes, one of the first anthraquinone derivatives used in painting is alizarin, a molecule which confers a red color with a blue undertone. Its vibrational properties have been studied by several authors [16–22], by means of Raman spectroscopy. The experimental spectra have been also assisted by density functional theory (DFT) calculations for the assignment of the vibrational modes and for modeling the molecular geometry [16,18,21]. Since Raman spectroscopy suffers from low sensitivity and the spectra of organic dyes could be worsened by the fluorescence background [10,23], surface enhanced Raman scattering (SERS) spectroscopy has been revealed as a useful technique to overcome these problems [16,24]. This is one of the reasons SERS spectroscopy is today applied to investigate samples of interest in chemistry, biology, medicine, cultural heritage, and other sectors [25–31].

SERS spectroscopy relys on the interaction between the molecule of interest (specially through heteroatoms such as N or O) and an appropriate substrate, to obtain a huge enhancement of the Raman signals. The molecule adsorbs on the substrate surface, which must contain high-reflective metals, such as silver, gold, or copper. The strong localization of the electromagnetic field associated with the collective excitation waves, usually called plasmons, of the electrons near the nanostructured metal surface, allows obtaining enhancements of several orders of magnitude (usually a factor up to 10^6) for the Raman signals of the adsorbed molecules. In addition to this mechanism, a chemical enhancement contribution, which usually provides Raman enhancement factor up to 10^2, can occur, which is essentially due to a charge transfer (CT) process between the adsorbed molecules and the metal substrates [32,33]. The formation of chemical interaction between the molecule and the active sites of the metal surface is also responsible for the perturbation of the

molecular polarizability, and therefore of vibrational frequency shifts, which provide useful information on the adsorption geometry of the molecule on the metal substrate [25–31].

Despite the large volume of experimental and theoretical data on alizarin (AZ), some questions are still open regarding the adsorption geometries on nanostructured silver substrates [10,12,17–19,22,24,34–37], especially in relation with the existence of different ionic species in solutions.

Therefore, in the present study, we re-analyzed the SERS spectra of AZ interacting with silver nanoparticles (AgNPs), by considering all the species present in solution at pH between 10 and 11. The adsorption of the different AZ species in solution on AgNPs determines the SERS spectral features, which have not been considered in detail in previous studies. The interpretation of the experimental findings was accomplished by performing DFT calculations, which represent a useful support for the interpretation of the SERS spectra [17–19,22].

Among the different metals, silver is one of the most computationally studied species. In particular, it has been observed that DFT calculations allow a correct determination of both the shift of the vibrational frequencies and the relative intensities when the analyte is adsorbed on a nanostructured surface modeled as Ag^+ or small charged silver clusters. This results should not be a surprise, because it has been experimentally ascertained that Ag(I) is present on nanostructured surfaces [38,39].

Moreover, it has been observed [40,41] that, in the first step of silver reduction, the formation of both $(Ag_3)^+$ and $(Ag_4)^{2+}$ occurs; consequently, for the first time, DFT calculations on the AZ^- (monoanionic) and AZ^{2-} (dianionic) species interacting with these clusters were carried out for the first time. It has been observed that DFT calculations performed on model systems made up by the adsorbate bound to a single Ag^+ or small charged cluster are suitable to simulate the active sites present on silver nanostructured surfaces [25,39,42,42–48]. This approach has been revealed able to faithfully reproduce the SERS spectral features of several systems [38,39,42,43,47,49–54], regarding both frequency positions and relative intensities, and to provide information on the chemical adsorption geometry. Therefore, the calculations in the present study aimed to model the adsorption geometry on silver nanoparticles of the different dye species in solution and to reproduce the measured SERS spectra.

2. Materials and Methods

2.1. Silver Nanoparticles Synthesis and Chemicals

The AgNPs were prepared by reducing $AgNO_3$ (99.9999% purity, Aldrich, Germany) with NH_2OH-HCl (99.9% purity, Aldrich) in extra-pure distilled water (HPLC grade, Lichrosolv, Merck) according to Leopold and Lendl procedure [55]. The pH value of the colloidal suspension was 10–11. AgNPs were remarkably stable, conserving their distinctive surface plasmon band centered at 409 nm for several weeks. AgNPs were activated before use by adding LiCl (>99% purity, Aldrich) 1 M aqueous solution [56,57] to a final concentration of 5×10^{-6} M (10 µL in 2 mL AgNPs dispersion). Alizarin (>99% purity, Aldrich) with 10^{-3} methanol (>99% purity, Merck) stock solution was added to the colloidal dispersion to reach the final concentrations of 2.5×10^{-6} and 1.2×10^{-5} M.

2.2. Instruments

Extinction spectra were recorded with a Cary60 UV-vis-NIR spectrophotometer (Agilent Technologies, S. Clara, CA, USA), with 2 nm bandwidth.

SERS spectra were measured with a MultiRAM FT-Raman spectrometer (Bruker, Germany) working in back scattering configuration, with excitation wavelength at 1064 nm. The resolution was set to 4 cm^{-1} and incident power was kept at 250 mW. The spectra were obtained by averaging 1000 scans.

2.3. Computational Details

Ab initio calculations within the DFT framework were performed with the Gaussian09 suite of programs [58] using the B3LYP exchange and correlation functional [59–61] along with the 6-311++G(d,p) basis set for all atoms but silver, which was described with the LANL2TZ basis set [62–65]. The molecular structure and the vibrational frequency calculations were carried out imposing a very tight criterion and an improved grid in the numerical evaluation of the integrals, INTEGRAL(GRID = 199974). It was verified that all the vibrational frequencies are real, confirming that the optimized structures are true minima [66].

The Raman and SERS intensities were obtained from the computed Raman activities, using the relationship [67–69]:

$$I_i = \frac{f(\nu_0 - \nu_i)^4 A_i}{\nu_i \left(1 - e^{\frac{-hc\nu_i}{k_B T}}\right)} \quad (1)$$

where I_i and A_i are the intensity and activity of the vibrational mode i, respectively; ν_0 is the exciting frequency (in cm^{-1}); ν_i is the vibrational frequency of the ith normal mode (in cm^{-1}); h, c, and k_B are fundamental constants; and f is a normalization factor for all peak intensities. The calculated spectra were reported by assigning to each normal mode a Lorentzian shape with a 25 cm^{-1} full width at half-maximum. The vibrational frequencies were scaled by a 0.981 factor, in agreement with previous calculation on anthraquinone [16].

3. Results and Discussion

Alizarin is an anthraquinone dye with the molecular structure shown in Figure 1a. Since we are interested in interpreting the results of SERS spectra of AZ at alkaline pH (between 10 and 11), a first important information is to state the existence in the pH range of the different species of this dye in solution. Cañamares et al. [18] established that the pK of alizarin are 5.25 and 11.5 to give rise to the AZ^- (monoanionic) and AZ^{2-} (dianionic) species, respectively. Moreover, Cañamares et al. [18] reported that the initial deprotonation of AZ^- is attributable to the loss of the H^+ ion by the oxygen atom bound to C2 (see Figure 1a for atom labeling).

Figure 1b shows the distribution diagram of the AZ, AZ^-, and AZ^{2-} species as a function of pH. In the experimental conditions of the SERS experiments, with a pH between 10 and 11, both AZ^- and AZ^{2-} species are present in the solution. This is the first useful information to select suitable models for the calculation of the SERS spectra.

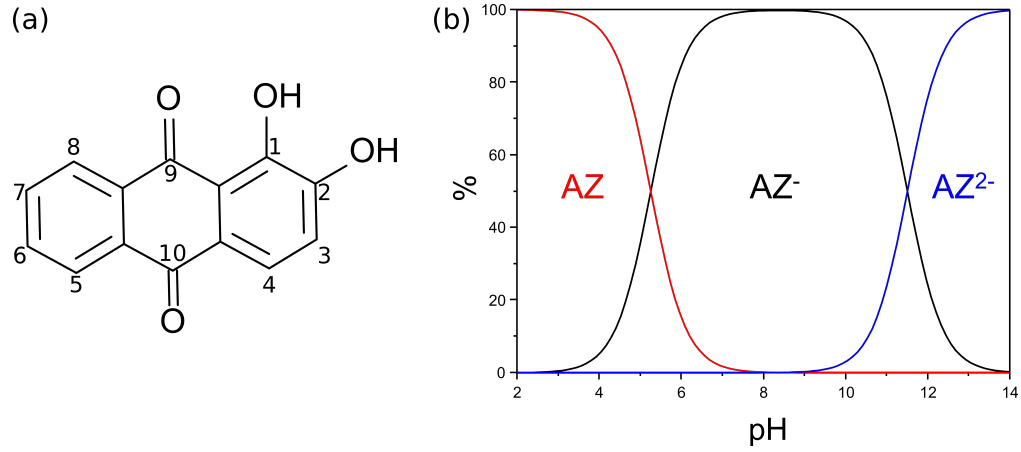

Figure 1. (**a**) Alizarin skeletal with atom labels. (**b**) Distribution diagram for alizarin species as a function of pH, for the $AZ/AZ^-/AZ^{2-}$ system. The two pK of AZ are 5.25 and 11.5, respectively.

The analysis of the electrostatic potential (shown in Figure 2) for AZ, AZ^- (with deprotonation on oxygen atoms bound to C1 or C2) and AZ^{2-} suggests that, if oxygen deprotonation

occurs on C1, AZ^- can interact as a bidentate ligand with metal substrate similarly to the models adopted in previous studies to interpret the AZ SERS spectra [17–19]. For completeness and to ascertain the correctness of the subsequent model of AZ^- with silver, the DFT calculations for both the structure optimizations and the vibrational frequencies were carried out considering also the deprotonation on C2. Finally, the calculation was performed also for AZ^{2-} species, and, for the first time, the SERS spectra were computed also for the interaction of AZ^{2-} with a silver cluster, as discussed in the following.

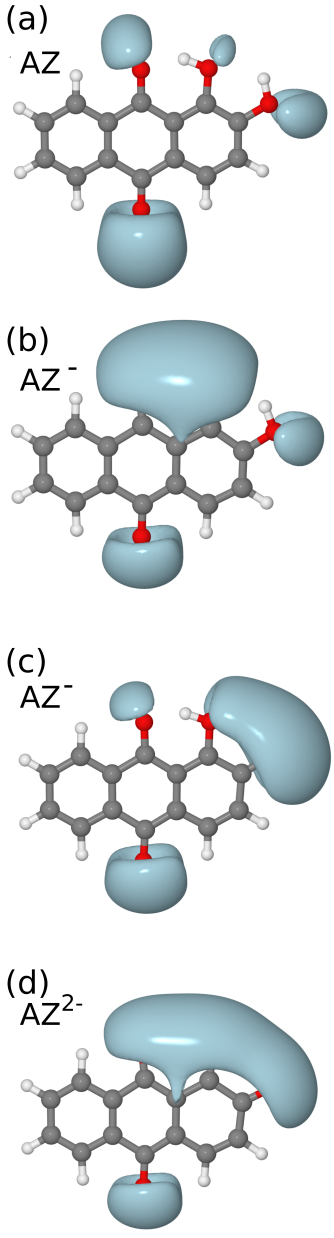

Figure 2. Electrostatic potential for: (**a**) AZ; (**b**) AZ^- with deprotonation on oxygen atom bound to C1; (**c**) AZ^- with deprotonation on oxygen atom bound to C2; and (**d**) AZ^{2-}. The C1 and C2 atom labels are reported in Figure 1a.

Regarding the substrate, it has been observed and it is now accepted that, during the silver reduction process for the formation of silver nanoparticles, the following reactions take place for the formation of charged species $(Ag_3)^+$ and $(Ag_4)^{2+}$ [40,41]:

$$Ag^+ + e^- \longrightarrow Ag \quad (2)$$

$$Ag^+ + Ag \longrightarrow (Ag_2)^+ \quad (3)$$

$$(Ag_2)^+ + Ag \longrightarrow (Ag_3)^+ \quad (4)$$

$$2(Ag_2)^+ \longrightarrow (Ag_4)^{2+} \quad (5)$$

The choice to use these silver cluster to model the substrate has been further corroborate by experimental finding [38,70]. It has been established that silver substrates have a sizable amount of Ag(I) on the surface, which acts as an active site on which the organic molecule can interact [38,70]. Therefore, the modeling of the metal surface was carried out considering the two clusters $(Ag_3)^+$ and $(Ag_4)^{2+}$, which, although not allowing to take into account the effect of the surface responsible for the electromagnetic enhancement of the Raman signals, proved to be suitable for reproducing the relative intensities and the observed shifts due to the chemical interaction in a whole series of molecules [38,42,49,50,53,54,71].

The accuracy of the calculations was initially verified by comparing the calculated vibrational frequencies of AZ with the assignment of Pagliai et al. [16], which is based on DFT calculations at B3LYP/6-31G(d) level; the assignment is an excellent starting point for the subsequent interpretation and discussion of the SERS spectra. The comparison is reported in Table 1 and it shows a good agreement of the computed vibrational frequencies with those of the assignment [16].

Table 1. Comparison of alizarin infrared and Raman vibrational frequencies computed at B3LYP/6-31G(d) [16] and B3LYP/6-311++G(d,p) level of theory (present work). The experimental infrared and Raman frequencies (in cm^{-1}) and assignment were taken from Cyranski et al. [21] and Pagliai et al. [16], respectively. The normal modes were labeled as ν for stretching, δ for in plane bending or deformation, γ for out of plane bending or deformation, and *sh* for shoulder.

	sym	B3LYP/6-31G(d) [16]	B3LYP/6-311++G(d,p)	IR	Raman	Assignment [16]
1	a''	47	43			$\gamma_{OH} + \gamma_{C-O} + \gamma_{C=O} + \gamma_{ring}$
2	a''	93	89			$\gamma_{OH} + \gamma_{C-O} + \gamma_{C=O} + \gamma_{ring}$
3	a''	123	116			$\gamma_{OH} + \gamma_{C-O} + \gamma_{C=O} + \gamma_{ring}$
4	a''	139	134			$\gamma_{OH} + \gamma_{C-O} + \gamma_{C=O} + \gamma_{ring}$
5	a''	178	176		182	$\gamma_{OH} + \gamma_{C-O} + \gamma_{C=O} + \gamma_{ring} + \gamma_{CH}$
6	a'	192	192		193	$\delta_{OH} + \delta_{C-O} + \delta_{C=O} + \delta_{ring} + \delta_{CH}$
7	a''	250	245		261	$\gamma_{CH} + \gamma_{C=O} + \gamma_{ring}$
8	a'	283	285		296	$\delta_{OH} + \delta_{C-O} + \delta_{C=O} + \delta_{ring} + \delta_{CH}$
9	a'	320	321			$\delta_{OH} + \delta_{C-O} + \delta_{C=O} + \delta_{ring} + \delta_{CH}$
10	a''	329	325			$\gamma_{OH} + \gamma_{C-O} + \gamma_{ring} + \gamma_{CH}$
11	a'	345	342		347	$\delta_{OH} + \delta_{C-O} + \delta_{C=O} + \delta_{CH}$
12	a'	385	386		392	$\delta_{OH} + \delta_{C=O} + \delta_{CH}$
13	a'	417	416		419	$\delta_{OH} + \delta_{C-O} + \delta_{C=O} + \delta_{ring} + \delta_{CH}$
14	a''	417	417	419		$\gamma_{CH} + \gamma_{ring}$
15	a''	444	440			$\gamma_{CH} + \gamma_{ring}$
16	a''	462	453			$\delta_{OH} + \delta_{C=O} + \delta_{ring}$
17	a'	475	465		470	$\delta_{OH} + \delta_{C-O} + \delta_{C=O} + \delta_{ring} + \delta_{CH}$
18	a'	478	477	486	486	$\gamma_{OH} + \gamma_{CH}$
19	a''	499	488	499	501	$\gamma_{OH} + \gamma_{CH}$
20	a''	562	564			$\gamma_{CH} + \gamma_{ring}$
21	a'	568	573	579		$\delta_{ring} + \delta_{OH}$
22	a'	608	615	620	620	$\delta_{CH} + \delta_{ring}$
23	a'	653	659		646	δ_{CH}
24	a''	656	666	660	662	$\gamma_{CH} + \gamma_{ring}$
25	a'	678	686	678	682	$\delta_{ring} + \delta_{OH} + \delta_{CH}$
26	a''	684	691	700		$\gamma_{CH} + \gamma_{OH}$
27	a''	712	719	712	710	$\gamma_{CH} + \gamma_{OH}$
28	a'	744	753	736		$\delta_{ring} + \delta_{OH}$
29	a''	768	767	748		$\gamma_{ring} + \gamma_{OH}$
30	a''	779	775	765	763	γ_{OH}

Table 1. *Cont.*

	sym	B3LYP/6-31G(d) [16]	B3LYP/6-311++G(d,p)	IR	Raman	Assignment [16]
31	a''	788	794	792	795	$\gamma_{CH} + \gamma_{OH}$
32	a'	825	828	828	830	$\delta_{ring} + \delta_{OH} + \delta_{CH}$
33	a''	840	846	848		γ_{CH}
34	a'	881	889	858		$\delta_{ring} + \delta_{CH}$
35	a''	896	899	895	895	γ_{CH}
36	a''	945	959	931		γ_{CH}
37	a''	965	984	955	960	γ_{CH}
38	a''	985	1000	972		γ_{CH}
39	a'	1006	1007	1012	1012	$\delta_{OH} + \delta_{CH} + \delta_{ring}$
40	a'	1024	1026	1031	1030	$\delta_{OH} + \delta_{CH}$
41	a'	1043	1046	1048	1048	$\delta_{OH} + \delta_{CH}$
42	a'	1085	1092	1102	1102	$\delta_{OH} + \delta_{CH}$
43	a'	1144	1149	1150*sh*	1150	$\delta_{OH} + \delta_{CH}$
44	a'	1156	1160	1160	1164	δ_{CH}
45	a'	1179	1182	1175		$\delta_{OH} + \delta_{CH}$
46	a'	1193	1193	1198	1191	$\delta_{OH} + \delta_{CH}$
47	a'	1227	1221	1220	1216	$\delta_{OH} + \delta_{CH}$
48	a'	1259	1261	1266	1270	$\delta_{OH} + \delta_{CH}$
49	a'	1284	1282	1295	1295*sh*	δ_{CH}
50	a'	1298	1293	1300*sh*	1300*sh*	$\delta_{OH} + \delta_{CH}$
51	a'	1327	1319		1330	$\delta_{OH} + \delta_{CH}$
52	a'	1337	1332	1332	1332	$\delta_{OH} + \delta_{CH} + \delta_{ring}$
53	a'	1359	1350	1350	1350	$\delta_{OH} + \delta_{CH}$
54	a'	1415	1405	1398	1399	$\delta_{OH} + \delta_{CH}$
55	a'	1454	1454	1429		δ_{CH}
56	a'	1465	1458	1452	1451	$\delta_{OH} + \delta_{CH}$
57	a'	1475	1476	1465	1463	$\delta_{CH} + \delta_{C=O}$
58	a'	1484	1486	1477	1481	$\delta_{OH} + \delta_{CH}$
59	a'	1578	1578	1571	1574	$\nu_{ring} + \delta_{CH}$
60	a'	1594	1592		1587	$\nu_{ring} + \delta_{OH} + \delta_{CH}$
61	a'	1597	1595	1589		$\nu_{ring} + \delta_{OH} + \delta_{CH}$
62	a'	1602	1601		1595	$\nu_{ring} + \delta_{OH}$
63	a'	1647	1641	1633	1632	$\nu_{C=O} + \delta_{OH}$
64	a'	1692	1685	1663	1658	$\delta_{OH} + \nu_{C=O}$
65	a'	3098	3111			ν_{CH}
66	a'	3112	3125			ν_{CH}
67	a'	3120	3130			ν_{CH}
68	a'	3130	3141			ν_{OH}
69	a'	3131	3143			ν_{CH}
70	a'	3133	3147			ν_{CH}
71	a'	3136	3224			ν_{CH}
72	a'	3568	3684			ν_{OH}

The calculations were also extended to different forms of alizarin, as shown by the vibrational frequencies and Raman activities reported in Tables S1–S4 and by the simulated Raman spectra in Figure 3. The spectra of the different species of alizarin in solution at the different pH values are a useful result to rationalize the variations which are observed experimentally by interaction of the dye with the metal substrate.

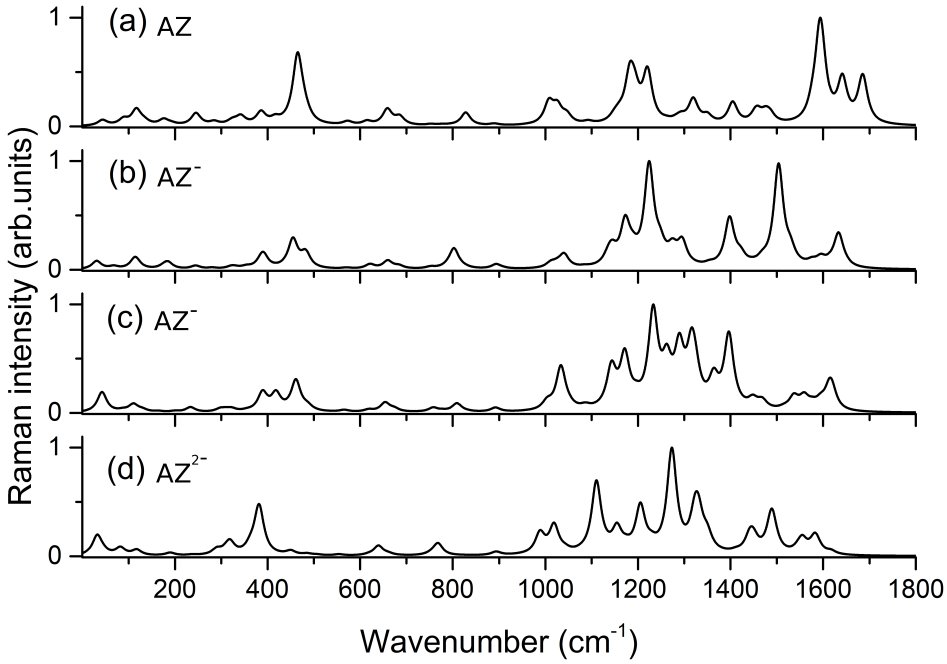

Figure 3. Computed Raman spectra for: (**a**) AZ; (**b**) AZ^{-} (deprotonation on the oxygen atom bound to C1); (**c**) AZ^{-} (deprotonation on the oxygen atom bound to C2); and (**d**) AZ^{2-}.

As stated above, the experimental SERS spectrum (shown in Figure 4) was measured at pH between 10 and 11 where AZ^{-} and AZ^{2-} coexist in solution. To simplify the analysis of SERS spectra and reduce the number of models to be used in the calculations, it was decided to perform the optimization and vibrational frequency calculations only for the AZ^{-} and AZ^{2-} species interacting with $(Ag_3)^{+}$ and $(Ag_4)^{2+}$ silver clusters, respectively. Therefore, the calculations were performed for globally neutral complexes.

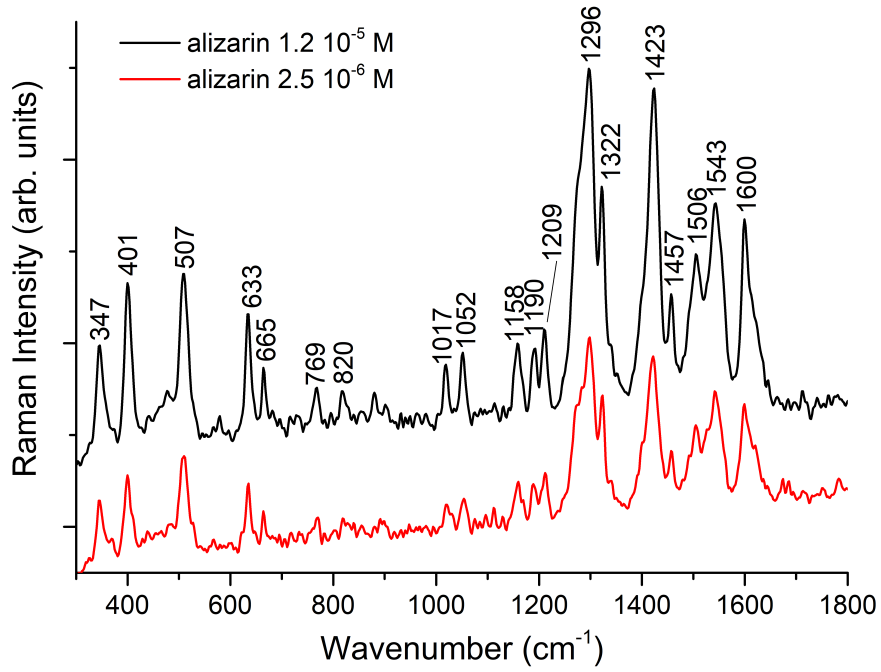

Figure 4. SERS spectra of alizarin. Excitation wavelength 1064 nm, 250 mW, 1000 scans. AgNP background has been subtracted.

The structures of the different optimized models are reported in Figure 5, while the simulated SERS spectra are shown in Figure 6. Depending on whether the dye is in the form AZ^{-} or AZ^{2-} and on the interaction of $(Ag_3)^{+}$ with the oxygen atoms, the calculated SERS spectra turn out to be different from each other. The different interaction of the $(Ag_3)^{+}$ cluster also leads to differences in simulated SERS spectra, but this can be an interesting aspect to more correctly describe adsorption geometry through a careful comparison between simulated and measured SERS spectra.

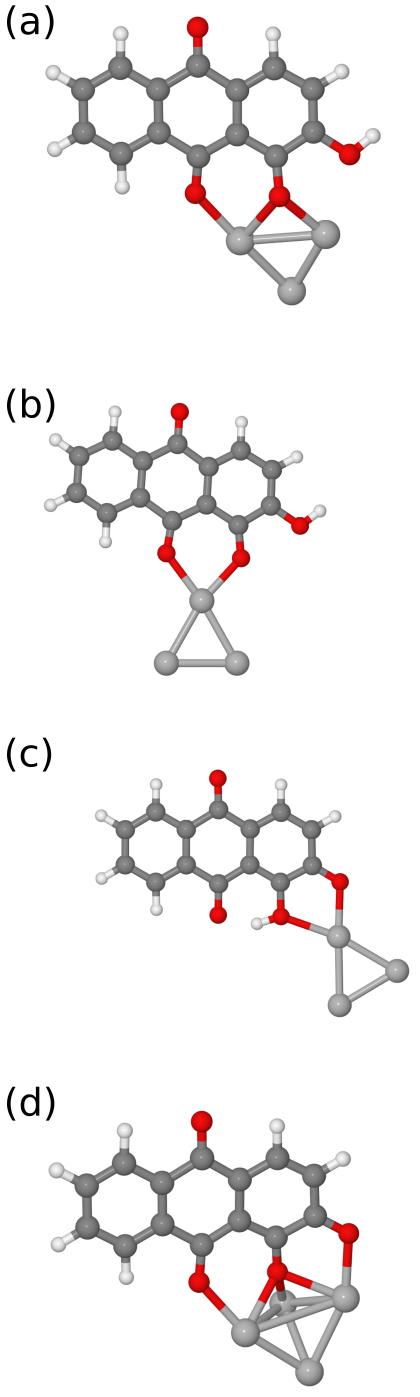

Figure 5. Optimized molecular structure of alizarin interacting as: AZ^{-} with $(Ag_3)^{+}$ cluster (**a**–**c**); and AZ^{2-} with $(Ag_4)^{2+}$ for (**d**).

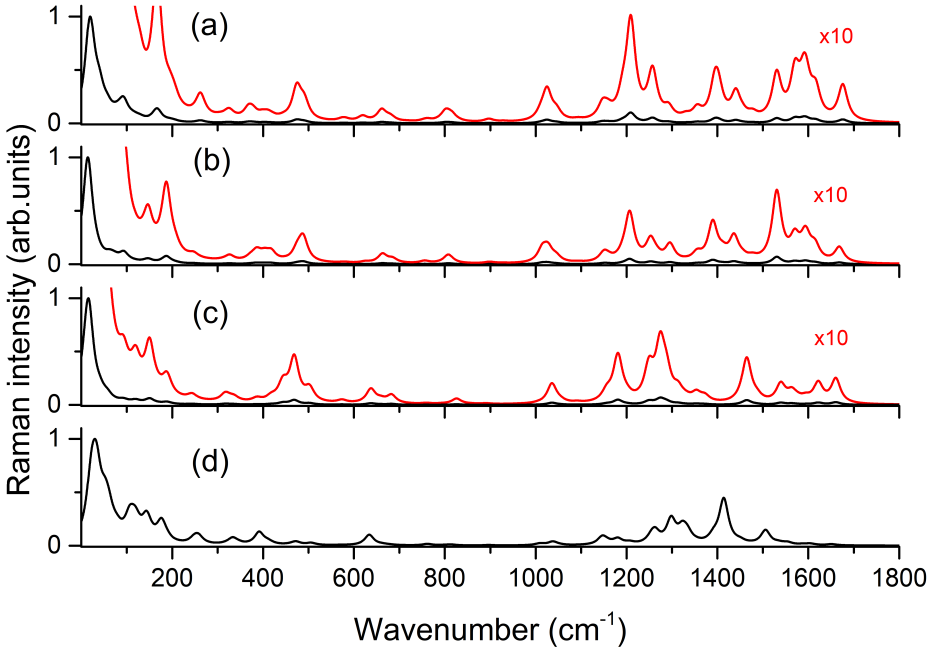

Figure 6. Black lines are the computed SERS spectra of alizarin interacting with silver clusters. The labels refer to models shown in Figure 5. Red lines are the 10× magnification of the respective black spectra.

All calculated frequencies are reported in Table S5–S7. Similar to the results reported by Cañamares et al. [18], the comparison between measured and simulated spectra in the frequency range between 0 and 1800 cm^{-1} can take advantage of the calculations on two different models. In the present study, the best agreement can be obtained by considering the simulated spectra for **a** and **d** models shown in Figure 5. In the latter, the interaction with silver involves oxygen atoms bound to C1, C2, and C9. This structure has not been taken into account in previous works to interpret the experimental spectra, but the calculated SERS spectrum faithfully reproduces most of the experimental features measured by some authors at alkaline pH [18,19,24,72]. However, a comparison between the measured SERS spectrum with those obtained by DFT calculations, as shown in Figure 7, suggests that this is not the only contribution to be taken into account. On the basis of the comparison, it is possible to note that the measured SERS spectrum can be faithfully reproduced considering in addition to the $AZ^{2-}/(Ag_4)^{2+}$ model also the contribution of AZ^{-} species interacting with $(Ag_3)^{+}$, confirming the importance to consider all the alizarin species (AZ^{-} and AZ^{2-}) present in solution. These results also provide important information on the adsorption geometry of the dye with metal substrate. In fact, the models adopted to simulate the SERS spectrum involve the interaction of alizarin through oxygen atoms bound to both C1 and C9 with the silver surface [17,18].

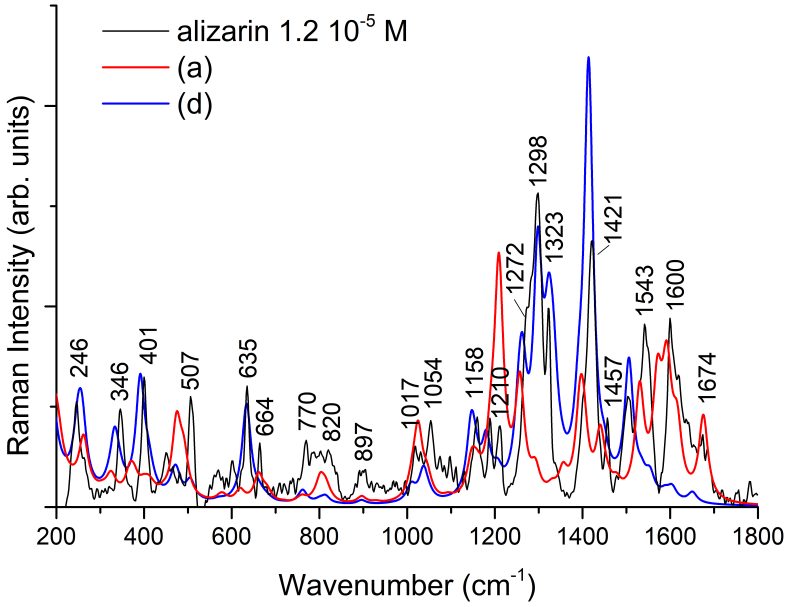

Figure 7. Comparison of the measured SERS spectra of alizarin with those calculated for the **a** and **d** models shown in Figure 5. The calculated intensities were uniformly scaled to match the experiment.

4. Conclusions

The SERS spectrum of alizarin at pH between 10 and 11 was re-interpreted on the basis of ab initio calculations in the framework of the density functional theory at the level B3LYP/6-311++G(d,p)/LanL2TZ. The active sites of the silver nanoparticles were modeled considering the clusters of $(Ag_3)^+$ and $(Ag_4)^{2+}$, which have already proved effective in reproducing the relative intensities in simulated SERS spectra of other systems [38,42,49,50,53,54,71]. The SERS spectrum of alizarin, due to the interaction between the two species of the dye in alkaline solution, AZ^- and AZ^{2-}, with silver nanoparticles was faithfully simulated with calculations on $AZ^-/(Ag_3)^+$ and $AZ^{2-}/(Ag_4)^{2+}$ to model the coexistence of these two species in solution. In fact, the final spectrum was achieved by properly adding the results of the calculations on either the complexes. The DFT calculations provided useful information on the adsorption geometry of alizarin on silver nanostructured surfaces, which allowed faithfully reproducing the experimental SERS spectrum.

Further insights on the adsorption geometry of AZ on silver surface could be theoretically achieved by performing calculations modeling the substrate with as slab or increasing the number of atoms [73–83] and experimentally by using other techniques such as X-ray photoelectron spectroscopy (XPS) and Near Edge X-Ray Absorption Fine Structure (NEXAFS) spectroscopy [38,39,43,84].

Supplementary Materials: The following are available online at https://www.mdpi.com/2079-4991/11/4/860/s1: Tables S1–S4: vibrational frequencies and Raman activities of simulated spectra shown in Figure 3; Tables S5–S8: vibrational frequencies and Raman activities of simulated spectra shown in Figure 6.

Author Contributions: Conceptualization, C.G. and M.P.; methodology, C.G. and M.P..; analysis, C.G., M.M. and M.P.; and data curation, C.G., M.M. and M.P. All authors have read and agreed to the published version of the manuscript.

Funding: This research received no external funding.

Acknowledgments: The authors thank MIUR-Italy ("Progetto Dipartimenti di Eccellenza 2018–2022" allocated to Department of Chemistry "Ugo Schiff") and Luca Conti for the figure of the distribution diagram.

Conflicts of Interest: The authors declare no conflict of interest.

References

1. Gettens, R.J.; Stout, G.L. *Painting Materials, a Short Encyclopaedia*; Dover Publications: New York, NY, USA, 1966.
2. Berrie, B.H. An Improved method for indentifying red lakes on art and historical artifacts. *Proc. Natl. Acad. Sci. USA* **2009**, *106*, 15095–15096. [CrossRef]
3. Kirby, J.; Spring, M.; Higgett, C. The Technology of Red Lake Pigment Manufacture: Study of the Dyestuff Substrate. *Nat. Gall. Tech. Bull.* **2005**, *26*, 71–88.
4. Kirby, J.; van Bommel, M.; Verhecken, A. (Eds.) *Natural Colorants for Dyeing and Lake Pigments: Practical Recipes and Their Historical Sources*; Archetype Publications: London, UK, 2014.
5. Osticioli, I.; Pagliai, M.; Comelli, D.; Schettino, V.; Nevin, A. Red lakes from Leonardo's Last Supper and other Old Master Paintings: Micro-Raman spectroscopy of anthraquinone pigments in paint cross-sections. *Spectrochim. Acta Part A Mol. Biomol. Spectrosc.* **2019**, *222*, 117273. [CrossRef] [PubMed]
6. Cardon, D. *Natural Dyes: Sources, Tradition, Technology and Science*; Archetype Publications: London, UK, 2007.
7. Kirby, J.; White, R. The identification of red lake pigment dyestuffs and a discussion of their use. *Nat. Gall. Tech. Bull.* **1996**, *17*, 56–80.
8. Wouters, J. High Performance Liquid Chromatography of Anthraquinones: Analysis of Plant and Insect Extracts and Dyed Textiles. *Stud. Conserv.* **1985**, *30*, 119–128. [CrossRef]
9. Murcia-Mascarós, S.; Domingo, C.; Sanchez-Cortes, S.; Cañamares, M.V.; Garcia-Ramos, J.V. Spectroscopic identification of alizarin in a mixture of organic red dyes by incorporation in Zr-Ormosil. *J. Raman Spectrosc.* **2005**, *36*, 420–426. [CrossRef]
10. Leona, M.; Stenger, J.; Ferloni, E. Application of surface-enhanced Raman scattering techniques to the ultrasensitive identification of natural dyes in works of art. *J. Raman Spectrosc.* **2006**, *37*, 981–992. [CrossRef]
11. Casadio, F.; Leona, M.; Van Duyne, J.R.L.R. Identification of Organic Colorants in Fibers, Paints, and Glazes by Surface Enhanced Raman Spectroscopy. *Acc. Chem. Res.* **2010**, *43*, 782–791. [CrossRef] [PubMed]
12. Leona, M. Microanalysis of organic pigments and glazes in polychrome works of art by surface-enhanced resonance Raman scattering. *Proc. Natl. Acad. Sci. USA* **2009**, *106*, 14757–14762. [CrossRef] [PubMed]
13. Whitney, A.V.; Casadio, F.; Van Duyne, R.P. Identification and Characterization of Artists' Red Dyes and Their Mixtures by Surface-Enhanced Raman Spectroscopy. *Appl. Spectrosc.* **2007**, *61*, 994–1000. [CrossRef]
14. Cañamares, M.V.; Leona, M. Surface-enhanced Raman scattering study of the red dye laccaic acid. *J. Raman Spectrosc.* **2007**, *38*, 1259–1266. [CrossRef]
15. Burgio, L.; Clark, R.J. Library of F-T Raman spectra of pigments, minerals, pigment media and varnishes, and supplement to existing library of Raman spectra of pigments with visible excitation. *Spectrochim. Acta* **2001**, *57A*, 1491–1521. [CrossRef]
16. Pagliai, M.; Osticioli, I.; Nevin, A.; Siano, S.; Cardini, G.; Schettino, V. DFT calculations of the IR and Raman spectra of anthraquinone dyes and lakes. *J. Raman Spectrosc.* **2018**, *49*, 668–683. [CrossRef]
17. Baran, A.; Wrzosek, B.; Bukowska, J.; Proniewicz, L.M.; Baranska, M. Analysis of alizarin by surface-enhanced and FT-Raman spectroscopy. *J. Raman Spectrosc.* **2009**, *40*, 436–441. [CrossRef]
18. Cañamares, M.V.; Garcia-Ramos, J.V.; Domingo, C.; Sanchez-Cortes, S. Surface-enhanced Raman scattering study of the adsorption of the anthraquinone pigment alizarin on Ag nanoparticles. *J. Raman Spectrosc.* **2004**, *35*, 921–927. [CrossRef]
19. Lofrumento, C.; Platania, E.; Ricci, M.; Becucci, M.; Castellucci, E.M. SERS Spectra of Alizarin Anion–Agn (n = 2, 4, 14) Systems: TDDFT Calculation and Comparison with Experiment. *J. Phys. Chem. C* **2016**, *120*, 12234–12241. [CrossRef]
20. Whitney, A.V.; Van-Duyne, R.P.; Casadio, F. An innovative surface-enhanced Raman spectroscopy (SERS) method for the identification of six historical red lakes and dyestuffs. *J. Raman Spectrosc.* **2006**, *37*, 993–1002. [CrossRef]
21. Cyrański, M.K.; Jamróz, M.H.; Rygula, A.; Dobrowolski, J.C.; Dobrzycki, L.; Baranska, M. On two alizarin polymorphs. *CrystEngComm* **2012**, *14*, 3667–3676. [CrossRef]
22. Lofrumento, C.; Platania, E.; Ricci, M.; Mulana, C.; Becucci, M.; Castellucci, E.M. The SERS spectra of alizarin and its ionized species: The contribution of the molecular resonance to the spectral enhancement. *J. Mol. Struct.* **2015**, *1090*, 98–106. [CrossRef]
23. Smith, E.; Dent, G. *Modern Raman Spectroscopy*; John Wiley & Sons, Ltd.: Chichester, UK, 2019.
24. Chen, K.; Leona, M.; Vo-Dinh, K.C.; Yan, F.; Wabuyele, M.B.; Vo-Dinh, T. Application of surface-enhanced Raman scattering (SERS) for the identification of anthraquinone dyes used in works of art. *J. Raman Spectrosc.* **2006**, *37*, 520–527. [CrossRef]
25. Aroca, R. *Surface-Enhanced Vibrational Spectroscopy*; Wiley & Sons: Chichester, UK, 2006.
26. Kneipp, K.; Moskovits, M.; Kneipp, H. *Surface-Enhanced Raman Scattering—Physics and Applications*; Springer: Berlin/Heidelberg, Germany, 2006.
27. Le Ru, E.C.; Etchegoin, P.G. *Principles of Surface-Enhanced Raman Spectroscopy and Related Plasmonic Effects*; Elsevier: Amsterdam, The Netherlands, 2009.
28. Schlücker, S. *Surface Enhanced Raman Spectroscopy: Analytical, Biophysical and Life Science Applications*; Wiley-VCH: Weinheim, Germany, 2011.
29. Procházka, M. *Surface-Enhanced Raman Spectroscopy, Bioanalytical, Biomolecular and Medical Applications*; Springer: Basel, Switzerland, 2016.
30. Fasolato, C. *Surface Enhanced Raman Spectroscopy for Biophysical Applications*; Springer: Berlin/Heidelberg, Germany, 2018.
31. Langer, J.; Jimenez de Aberasturi, D.; Aizpurua, J.; Alvarez-Puebla, R.A.; Auguié, B.; Baumberg, J.J.; Bazan, G.C.; Bell, S.E.J.; Boisen, A.; Brolo, A.G.; et al. Present and Future of Surface-Enhanced Raman Scattering. *ACS Nano* **2020**, *14*, 28–117. [CrossRef]

32. Lombardi, J.R.; Birke, R.L. A Unified Approach to Surface-Enhanced Raman Spectroscopy. *J. Phys. Chem. C* **2008**, *112*, 5605–5617. [CrossRef]
33. Lombardi, J.R.; Birke, R.L. A Unified View of Surface-Enhanced Raman Scattering. *Acc. Chem. Res.* **2009**, *42*, 734–742. [CrossRef] [PubMed]
34. Cañamares, M.V.; Garcia-Ramos, J.V.; Gómez-Varga, J.D.; Domingo, C.; Sanchez-Cortes, S. Ag Nanoparticles Prepared by Laser Photoreduction as Substrates for in Situ Surface-Enhanced Raman Scattering Analysis of Dyes. *Langmuir* **2007**, *23*, 5210–5215. [CrossRef] [PubMed]
35. Retko, K.; Ropret, P.; Cerc Korošec, R.; Sanchez-Cortes, S.; Cañamares, M.V. Characterization of HPC-based photoreduced SERS substrates and detection of different organic dyes. *J. Raman Spectrosc.* **2018**, *49*, 1288–1300. [CrossRef]
36. Marcaida, I.; Maguregui, M.; Morillas, H.; García-Florentino, C.; Pintus, V.; Aguayo, T.; Campos-Vallette, M.; Madariaga, J.M. Optimization of sample treatment for the identification of anthraquinone dyes by surface-enhanced Raman spectroscopy. *Anal. Bioanal. Chem.* **2017**, *409*, 2221–2228. [CrossRef] [PubMed]
37. Pozzi, F.; Zaleski, S.; Casadio, F.; Van Duyne, R.P. SERS Discrimination of Closely Related Molecules: A Systematic Study of Natural Red Dyes in Binary Mixtures. *J. Phys. Chem. C* **2016**, *120*, 21017–21026. [CrossRef]
38. Pagliai, M.; Caporali, S.; Muniz-Miranda, M.; Pratesi, G.; Schettino, V. SERS, XPS, and DFT Study of Adenine Adsorption on Silver and Gold Surfaces. *J. Phys. Chem. Lett.* **2012**, *3*, 242–245. [CrossRef] [PubMed]
39. Pagliai, M.; Muniz-Miranda, F.; Schettino, V.; Muniz-Miranda, M. Competitive Solvation and Chemisorption in Silver Colloidal Suspensions. In *UK Colloids 2011*; Starov, V., Griffiths, P., Eds.; Springer: Berlin/Heidelberg, Germany 2012; pp. 39–44.
40. Lawless, D.; Kapoor, S.; Kennepohl, P.; Meisel, D.; Serpone, N. Reduction and Aggregation of Silver Ions at the Surface of Colloidal Silica. *J. Phys. Chem.* **1994**, *98*, 9619–9625. [CrossRef]
41. Xiong, Y.; Washio, I.; Chen, J.; Sadilek, M.; Xia, Y. Trimeric Clusters of Silver in Aqueous $AgNO_3$ Solutions and Their Role as Nuclei in Forming Triangular Nanoplates of Silver. *Angew. Chem. Int. Ed.* **2007**, *46*, 4917–4921. [CrossRef] [PubMed]
42. Muniz-Miranda, M.; Pagliai, M.; Muniz-Miranda, F.; Schettino, V. Raman and computational study of solvation and chemisorption of thiazole in silver hydrosol. *Chem. Commun.* **2011**, *47*, 3138–3140. [CrossRef] [PubMed]
43. Muniz-Miranda, F.; Pedone, A.; Muniz-Miranda, M. Raman and Computational Study on the Adsorption of Xanthine on Silver Nanocolloids. *ACS Omega* **2018**, *3*, 13530–13537. [CrossRef] [PubMed]
44. Owen, A.R.; Golden, J.W.; Price, A.S.; Henry, W.A.; Barker, W.K.; Perry, D.A. Surface-Enhanced Vibrational Spectroscopy and Density Functional Theory Study of Isoniazid Layers Adsorbed on Silver Nanostructures. *J. Phys. Chem. C* **2014**, *118*, 28959–28969. [CrossRef]
45. Jensen, L.; Aikens, C.M.; Schatz, G.C. Electronic structure methods for studying surface-enhanced Raman scattering. *Chem. Soc. Rev.* **2008**, *37*, 1061–1073. [CrossRef] [PubMed]
46. Otto, A. The 'chemical' (electronic) contribution to surface-enhanced Raman scattering. *J. Raman Spectrosc.* **2005**, *36*, 497–509. [CrossRef]
47. Aranda, D.; Valdivia, S.; Soto, J.; López-Tocón, I.; Avila, F.J.; Otero, J.C. Theoretical Approaches for Modeling the Effect of the Electrode Potential in the SERS Vibrational Wavenumbers of Pyridine Adsorbed on a Charged Silver Surface. *Front. Chem.* **2019**, *7*, 423. [CrossRef] [PubMed]
48. Roy, D.; Furtak, T.E. Vibrational characteristics of silver clusters in surface-enhanced Raman scattering. *Phys. Rev. B* **1986**, *34*, 5111–5117. [CrossRef] [PubMed]
49. Muniz-Miranda, M.; Pagliai, M. Positively Charged Active Sites for the Adsorption of Five-Membered Heterocycles on Silver Colloids. *J. Phys. Chem. C* **2013**, *117*, 2328–2333. [CrossRef]
50. Muniz-Miranda, M.; Pagliai, M.; Cardini, G.; Schettino, V. Role of Surface Metal Clusters in SERS Spectra of Ligands Adsorbed on Ag Colloidal Nanoparticles. *J. Phys. Chem. C* **2008**, *112*, 762–767. [CrossRef]
51. Huang, R.; Zhao, L.B.; Wu, D.Y.; Tian, Z.Q. Tautomerization, Solvent Effect and Binding Interaction on Vibrational Spectra of Adenine–Ag+ Complexes on Silver Surfaces: A DFT Study. *J. Phys. Chem. C* **2011**, *115*, 13739–13750. [CrossRef]
52. Yao, G.; Zhai, Z.; Zhong, J.; Huang, Q. DFT and SERS Study of 15N Full-Labeled Adenine Adsorption on Silver and Gold Surfaces. *J. Phys. Chem. C* **2017**, *121*, 9869–9878. [CrossRef]
53. Cardini, G.; Muniz-Miranda, M.; Pagliai, M.; Schettino, V. A density functional study of the SERS spectra of pyridine adsorbed on silver clusters. *Theor. Chem. Acc.* **2007**, *117*, 451–458. [CrossRef]
54. Pagliai, M.; Muniz-Miranda, M.; Cardini, G.; Schettino, V. Solvation Dynamics and Adsorption on Ag Hydrosols of Oxazole: A Raman and Computational Study. *J. Phys. Chem. A* **2009**, *113*, 15198–15205. [CrossRef] [PubMed]
55. Leopold, N.; Lendl, B. A New Method for Fast Preparation of Highly Surface-Enhanced Raman Scattering (SERS) Active Silver Colloids at Room Temperature by Reduction of Silver Nitrate with Hydroxylamine Hydrochloride. *J. Phys. Chem. B* **2003**, *107*, 5723–5727. [CrossRef]
56. Giorgetti, E.; Marsili, P.; Giammanco, F.; Trigari, S.; Gellini, C.; Muniz-Miranda, M. Ag nanoparticles obtained by pulsed laser ablation in water: Surface properties and SERS activity. *J. Raman Spectrosc.* **2015**, *46*, 462–469. [CrossRef]
57. Koo, T.W.; Chan, S.; Sun, L.; Su, X.; Zhang, J.; Berlin, A.A. Specific Chemical Effects on Surface-Enhanced Raman Spectroscopy for Ultra-Sensitive Detection of Biological Molecules. *Appl. Spectrosc.* **2004**, *58*, 1401–1407. [CrossRef] [PubMed]
58. Frisch, M.J.; Trucks, G.W.; Schlegel, H.B.; Scuseria, G.E.; Robb, M.A.; Cheeseman, J.R.; Scalmani, G.; Barone, V.; Mennucci, B.; Petersson, G.A.; et al. *Gaussian 09, Revision C.01*; Gaussian, Inc.: Wallingford, CT, USA, 2010.

59. Becke, A.D. Density-functional thermochemistry. III. The role of exact exchange. *J. Chem. Phys.* **1993**, *98*, 5648–5652. [CrossRef]
60. Lee, C.; Yang, W.; Parr, R.G. Development of the Colle-Salvetti correlation-energy formula into a functional of the electron density. *Phys. Rev. B* **1988**, *37*, 785–789. [CrossRef]
61. Vosko, S.H.; Wilk, L.; Nusair, M. Accurate spin-dependent electron liquid correlation energies for local spin density calculations: A critical analysis. *Can. J. Phys.* **1980**, *58*, 1200–1211. [CrossRef]
62. Hay, P.J.; Wadt, W.R. Ab initio effective core potentials for molecular calculations. Potentials for K to Au including the outermost core orbitals. *J. Chem. Phys.* **1985**, *82*, 299–310. [CrossRef]
63. Roy, L.E.; Hay, P.J.; Martin, R.L. Revised Basis Sets for the LANL Effective Core Potentials. *J. Chem. Theory Comput.* **2008**, *4*, 1029–1031. [CrossRef] [PubMed]
64. Pritchard, B.P.; Altarawy, D.; Didier, B.; Gibson, T.D.; Windus, T.L. New Basis Set Exchange: An Open, Up-to-Date Resource for the Molecular Sciences Community. *J. Chem. Inf. Model.* **2019**, *59*, 4814–4820. [CrossRef] [PubMed]
65. Feller, D. The role of databases in support of computational chemistry calculations. *J. Comput. Chem.* **1996**, *17*, 1571–1586. [CrossRef]
66. Baker, J. Molecular Structure and Vibrational Spectra. In *Handbook of Computational Chemistry*; Leszczynski, J., Ed.; Springer: Dordrecht, The Netherlands, 2012; pp. 293–359. [CrossRef]
67. Polavarapu, P.L. Ab initio vibrational Raman and Raman optical activity spectra. *J. Phys. Chem.* **1990**, *94*, 8106–8112. [CrossRef]
68. Keresztury, G.; Holly, S.; Besenyei, G.; Varga, J.; Wang, A.; Durig, J. Vibrational spectra of monothiocarbamates-II. IR and Raman spectra, vibrational assignment, conformational analysis and ab initio calculations of S-methyl-N,N-dimethylthiocarbamate. *Spectrochim. Acta A Mol. Biomol. Spectrosc.* **1993**, *49*, 2007–2026. [CrossRef]
69. Krishnakumar, V.; Keresztury, G.; Sundius, T.; Seshadri, S. Density functional theory study of vibrational spectra and assignment of fundamental vibrational modes of 1-methyl-4-piperidone. *Spectrochim. Acta A Mol. Biomol. Spectrosc.* **2007**, *68*, 845–850. [CrossRef] [PubMed]
70. Muniz-Miranda, M.; Caporali, S. Surface-enhanced Raman scattering of 'push–pull' molecules: Disperse orange 3 adsorbed on Au and Ag nanoparticles. *J. Opt.* **2015**, *17*, 114005. [CrossRef]
71. Muniz-Miranda, M.; Cardini, G.; Pagliai, M.; Schettino, V. DFT investigation on the SERS band at $\sim$1025cm^{-1} of pyridine adsorbed on silver. *Chem. Phys. Lett.* **2007**, *436*, 179–183. [CrossRef]
72. Van Elslande, E.; Lecomte, S.; Le Hô, A.S. Micro-Raman spectroscopy (MRS) and surface-enhanced Raman scattering (SERS) on organic colourants in archaeological pigments. *J. Raman Spectrosc.* **2008**, *39*, 1001–1006. [CrossRef]
73. Van Dyck, C.; Fu, B.; Van Duyne, R.P.; Schatz, G.C.; Ratner, M.A. Deducing the Adsorption Geometry of Rhodamine 6G from the Surface-Induced Mode Renormalization in Surface-Enhanced Raman Spectroscopy. *J. Phys. Chem. C* **2018**, *122*, 465–473. [CrossRef]
74. Ungurean, A.; Oltean, M.; David, L.; Leopold, N.; Prates Ramalho, J.P.; Chiş, V. Adsorption of sulfamethoxazole molecule on silver colloids: A joint SERS and DFT study. *J. Mol. Struct.* **2014**, *1073*, 71–76. [CrossRef]
75. Reckien, W.; Kirchner, B.; Janetzko, F.; Bredow, T. Theoretical Investigation of Formamide Adsorption on Ag(111) Surfaces. *J. Phys. Chem. C* **2009**, *113*, 10541–10547. [CrossRef]
76. Zhao, L.L.; Jensen, L.; Schatz, G.C. Pyridine-Ag20 Cluster: A Model System for Studying Surface-Enhanced Raman Scattering. *J. Am. Chem. Soc.* **2006**, *128*, 2911–2919. [CrossRef] [PubMed]
77. Zhao, L.L.; Jensen, L.; Schatz, G.C. Surface-Enhanced Raman Scattering of Pyrazine at the Junction between Two Ag20 Nanoclusters. *Nano Lett.* **2006**, *6*, 1229–1234. [CrossRef] [PubMed]
78. Jensen, L.; Zhao, L.L.; Schatz, G.C. Size-Dependence of the Enhanced Raman Scattering of Pyridine Adsorbed on Agn (n = 2–8, 20) Clusters. *J. Phys. Chem. C* **2007**, *111*, 4756–4764. [CrossRef]
79. Birke, R.L.; Znamenskiy, V.; Lombardi, J.R. A charge-transfer surface enhanced Raman scattering model from time-dependent density functional theory calculations on a Ag10-pyridine complex. *J. Chem. Phys.* **2010**, *132*, 214707. [CrossRef] [PubMed]
80. Tsuneda, T.; Iwasa, T.; Taketsugu, T. Roles of silver nanoclusters in surface-enhanced Raman spectroscopy. *J. Chem. Phys.* **2019**, *151*, 094102. [CrossRef] [PubMed]
81. Arenas, J.F.; Soto, J.; Tocón, I.L.; Fernández, D.J.; Otero, J.C.; Marcos, J.I. The role of charge-transfer states of the metal-adsorbate complex in surface-enhanced Raman scattering. *J. Chem. Phys.* **2002**, *116*, 7207–7216. [CrossRef]
82. Avila, F.; Ruano, C.; Lopez-Tocon, I.; Arenas, J.F.; Soto, J.; Otero, J.C. How the electrode potential controls the selection rules of the charge transfer mechanism of SERS. *Chem. Commun.* **2011**, *47*, 4213–4215. [CrossRef] [PubMed]
83. Avila, F.; Fernandez, D.J.; Arenas, J.F.; Otero, J.C.; Soto, J. Modelling the effect of the electrode potential on the metal–adsorbate surface states: Relevant states in the charge transfer mechanism of SERS. *Chem. Commun.* **2011**, *47*, 4210–4212. [CrossRef] [PubMed]
84. Diller, K.; Maurer, R.J.; Müller, M.; Reuter, K. Interpretation of X-ray absorption spectroscopy in the presence of surface hybridization. *J. Chem. Phys.* **2017**, *146*, 214701. [CrossRef] [PubMed]